

# An improved pore-network model including viscous coupling effects using direct simulation by the lattice Boltzmann method



Chiyu Xie<sup>a</sup>, Ali Q. Raeini<sup>b</sup>, Yihang Wang<sup>a</sup>, Martin J. Blunt<sup>b,\*</sup>, Moran Wang<sup>a,\*</sup>

<sup>a</sup> Department of Engineering Mechanics and CNMM, Tsinghua University, Beijing 100084, China

<sup>b</sup> Department of Earth Science & Engineering, Imperial College London, London SW7 2AZ, UK

## ARTICLE INFO

### Article history:

Received 29 July 2016

Revised 24 November 2016

Accepted 28 November 2016

Available online 30 November 2016

### Keywords:

Pore-network model

Viscous coupling effect

Two-phase flow

Lattice Boltzmann method

Porous media

## ABSTRACT

Viscous coupling during simultaneous flow of different fluid phases has a significant impact on their flow through porous media. In this work, a new multiscale strategy is proposed for multiphase flow in porous media. We use the lattice Boltzmann method (LBM) to simulate two-phase flow at pore scale and obtain empirical terms for the viscous coupling inside individual pores. The empirical coupling terms are then used in a pore-network model to efficiently simulate two-phase flow through porous media at core scale. It is shown that including viscous coupling leads to better predictions of relative permeability.

© 2016 Elsevier Ltd. All rights reserved.

## 1. Introduction

The understanding of multiphase flow at pore scale is important for many applications, including carbon dioxide storage, petroleum recovery and the exploitation of shale oil and gas (Blunt et al., 2013). Pore-scale modeling is important to develop this understanding for two reasons: (1) it provides physical insight into displacement processes which is missing from empirical continuum formulations of fluid flow (Joekar-Niasar and Hassanizadeh, 2012); and (2) it acts as a complement to laboratory experiments, providing rapid predictions of properties for a range of flow conditions (Raeini et al., 2014).

Among various pore-scale simulators, pore-network models are extremely efficient and have been extensively used to study fluid flow through porous media (Joekar-Niasar and Hassanizadeh, 2012; Blunt, 2001). The idealization of the pore space as a lattice of pores connected by throats was first advanced by Fatt (Fatt, 1956). Then, the use of geologically realistic networks was introduced by Bryant and Blunt (Bryant and Blunt, 1992) and Bryant et al. (Bryant et al., 1993a,b). Bakke and Øren (Bakke and Øren, 1997) further extended this method to represent a wide range of sedimentary rocks. Patzek (Patzek, 2001) presented a series of accurate predictions of multiphase flow properties using this approach. Network models can accommodate different rock wettabilities

(Øren and Bakke, 2003; Valvatne and Blunt, 2004; Ryazanov et al., 2010) and three-phase flow (Fenwick and Blunt, 1998; Van et al., 2004; Piri and Blunt, 2005a,b).

Despite the success and wide application of network modeling, it still suffers from some limitations. The major problem is the simplification of the pore-space geometry and flow processes within it, which then leads to the neglect of important effects, such as viscous coupling (Valvatne and Blunt, 2004), which is usually of great importance (Ehrlich, 1993).

To overcome these limitations, it is necessary to perform simulations that solve the relevant flow equations directly on a representation of the pore space. The lattice Boltzmann method (LBM) is widely used since it can handle multiphase fluid transport in complex structures coupled with interfacial dynamics, electrokinetics and thermodynamics (He and Li, 2000; Wang, 2012; Guo and Wang, 2015; Xie et al., 2015; Chen and Doolen, 1998; Aidun and Clausen, 2010; Huang et al., 2015). Various types of LBMs have been employed to perform direct simulations of two-phase flow in porous media, including both capillary and viscous forces (Liu et al., 2015; Gunstensen et al., 1991; Shan and Chen, 1993; Swift et al., 1995; He et al., 1999; Inamuro et al., 2004; Lee and Lin, 2005; Zheng et al., 2006; Connington and Lee, 2013; Shao et al., 2014; Vogel et al., 2005; Ahrenholz et al., 2008; Lehmann et al., 2008). Huang et al. (Huang et al., 2009a) and Li et al. (Li et al., 2005) found that viscous coupling effects – how the flow of one phase impacts the other – are important over a broad range of relevant flow conditions. However, the computational cost of LBM, or indeed any other direct simulation approach, to study flow in

\* Corresponding authors.

E-mail addresses: [m.blunt@imperial.ac.uk](mailto:m.blunt@imperial.ac.uk) (M.J. Blunt), [mrwang@tsinghua.edu.cn](mailto:mrwang@tsinghua.edu.cn) (M. Wang).

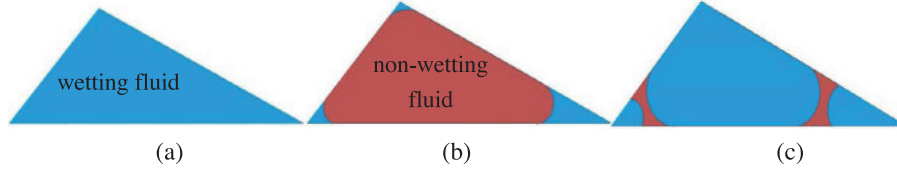


**Fig. 1.** Possible fluid configurations. (a) Wetting fluid filled the whole pore. (b) Wetting fluid in the corner with the non-wetting phase in the center. (c) One fluid layers (red) sandwiched between the other fluid occupying the corner and center. (For interpretation of the references to color in this figure legend, the reader is referred to the web version of this article.)

realistic rock samples to derive averaged flow properties at the mm to cm scale, is extremely huge, and for complex systems, it is difficult to accommodate all the relevant flow physics and the pore geometry in a single direct simulation.

In this work, we combine the advantages of both the lattice Boltzmann method and pore-network modeling: conceptually we consider the network model as an upscaled representation of flow with properties derived from a pore-scale LBM simulation. We will update a two-phase network model (Valvatne and Blunt, 2004) while employing an improved free-energy multiphase LBM model for the direct simulations (Zheng et al., 2006; Shao et al., 2014). Then the effect of viscous coupling will be rigorously considered by lattice Boltzmann simulations in the pore space. Furthermore, two empirical functions will be obtained using our LBM results and used to include the effect of viscous coupling in a previous pore-network model (Valvatne et al., 2005).

## 2. Methodology

In pore-network model (Valvatne and Blunt, 2004), flow conductance  $g_p$  of fluid  $p$  is the key parameter to estimate transport properties like flow rate  $q_p$  and relative permeability  $k_{rp}$ . The local flow rates  $q_{p,ij}$  between each pair of adjacent pores  $i$  and  $j$  are generalized by Darcy's law as

$$q_{p,ij} = g_{p,ij} \nabla P_{ij}, \quad (1)$$

where  $\nabla P_{ij}$  is the pressure gradient between the pore centers. For different fluid configurations shown in Fig. 1, the conductance  $g_p$  is decided accordingly.

The single-phase conductance is given by

$$g_p = \lambda \frac{A^2 G}{\mu_p}, \quad (2)$$

with parameter  $\lambda$  being 0.5, 0.6 and 0.5623 for circular, triangular and square elements respectively (Oren et al., 1998; Patzek and Silin, 2001).  $\mu$  is the dynamic viscosity,  $A$  is the cross-sectional area, and  $G$  is the shape factor (Mason and Morrow, 1991).

For two-phase flow, the conductance of each phase should be computed separately. For fluids occupying the corner and layer area, empirical expressions (Valvatne and Blunt, 2004) are adopted as

$$g_{p,c} = C \frac{A_c^2 G_c}{\mu_c}, \quad (3)$$

$$g_{p,l} = \frac{b_0^4 \tilde{g}_l}{\mu_l}, \quad (4)$$

where subscripts  $c$  and  $l$  represent the corner and layer configurations respectively, parameters  $C$ ,  $A_c$  and  $G_c$  are all related with the corner fluid geometry, while  $b_0$  and  $\tilde{g}_l$  are geometry parameters of the layer fluid.

It is noted that Eqs. (3) and (4) are derived for two-phase case but only the viscosity of one phase appears in each equation, which means that flow in each phase is independent of the other phase and viscous coupling effect is not considered.

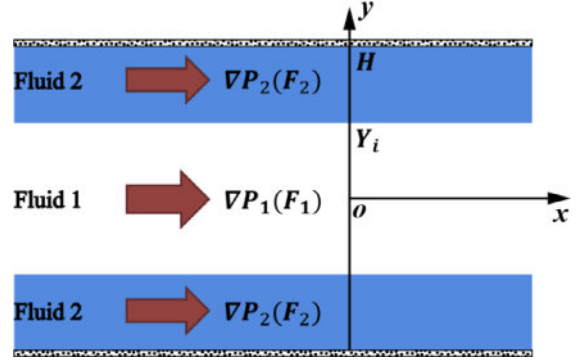


**Fig. 2.** Sketch of two-phase co-current flow between two infinite and parallel plates.

However, the existence of the other phase should not be ignored as illustrated in the following example, in which two-phase co-current flow inside a straight channel formed between two infinite and parallel plates is considered. As shown in Fig. 2, fluid 1 with density  $\rho_1$  and kinematic viscosity  $\nu_1$  lays symmetrically in the center driven by pressure gradient  $\nabla P_1$ , while fluid 2 with density  $\rho_2$  and kinematic viscosity  $\nu_2$  lays in two sides close to the plates driven by pressure gradient  $\nabla P_2$ . The distance between two plates is  $2H$ , with interface coordinates being  $\pm Y_i$ . Theoretical cross-sectional velocity distribution is obtained as (Huang and Lu, 2009)

$$0 \leq y < Y_i: \quad u = A_1 y^2 + C_1 \quad (5a)$$

$$Y_i \leq y \leq H: \quad u = A_2 y^2 + B_2 y + C_2, \quad (5b)$$

where

$$A_1 = -\nabla P_1 / (2\rho_1 \nu_1) \quad (6a)$$

$$A_2 = -\nabla P_2 / (2\rho_2 \nu_2) \quad (6b)$$

$$B_2 = -2A_2 Y_i + 2A_1 Y_i (\rho_1 \nu_1) / (\rho_2 \nu_2) \quad (6c)$$

$$C_1 = (A_2 - A_1) Y_i^2 - B_2 (H - Y_i) - A_2 H^2 \quad (6d)$$

$$C_2 = -A_2 H^2 - B_2 H. \quad (6e)$$

When applying the same pressure gradient as  $\nabla P_1 = \nabla P_2 = \nabla P$ , the conductance of both fluids are derived as

$$0 \leq y < Y_i: \quad g_1 = \frac{1}{H \nabla P} \int_0^{Y_i} u dy = \frac{Y_i^3}{3H\rho_1 \nu_1} + \frac{Y_i(H^2 - Y_i^2)}{2H\rho_2 \nu_2} \quad (7a)$$

$$Y_i \leq y \leq H: \quad g_2 = \frac{1}{H \nabla P} \int_{Y_i}^H u dy = \frac{1}{\rho_2 \nu_2} \left( \frac{H^2}{3} + \frac{Y_i^3}{6H} - \frac{HY_i}{2} \right). \quad (7b)$$

It is clear from the above equation that the conductance of fluid 1 is affected by fluid 2 for this simple cross-flow configuration, which demonstrates the importance of viscous coupling effect when estimating two-phase transport properties. For other types of configurations in pore-network models, however, analytical solutions are very difficult to obtain, and the viscous coupling between phases becomes much more complex.

In this paper, we adopt direct simulation by a free-energy based multiphase LB model (Zheng et al., 2006; Shao et al., 2014). Two sets of LB equations are derived for the evolution of two-phase momentum and interfacial dynamics respectively as

$$f_i(\mathbf{x} + \mathbf{c}_i \Delta t, t + \Delta t) - f_i(\mathbf{x}, t) = -\frac{1}{\tau_f} (f_i(\mathbf{x}, t) - f_i^{eq}(\mathbf{x}, t)) + \Omega'_f, \quad (8)$$

$$g_i(\mathbf{x} + \mathbf{c}_i \Delta t, t + \Delta t) - g_i(\mathbf{x}, t) = -\frac{1}{\tau_g} (g_i(\mathbf{x}, t) - g_i^{eq}(\mathbf{x}, t)), \quad (9)$$

with the collision term ( $\Omega'_f$ ) given as

$$\Omega'_f = \left( 1 - \frac{1}{2\tau_f} \right) \frac{3\Delta t \omega_i}{c^2} \times (\mathbf{c}_i - \mathbf{u}) \cdot \left[ \nabla \left( \frac{\rho c^2}{3} \right) \Gamma_i + (-\phi \nabla \mu + \mathbf{F})(1 + \Gamma_i) \right], \quad (10)$$

$$\Gamma_i = \frac{3\mathbf{c}_i \cdot \mathbf{u}}{c^2} + \frac{9(\mathbf{c}_i \cdot \mathbf{u})^2}{2c^4} - \frac{3\mathbf{u} \cdot \mathbf{u}}{c^2}, \quad (11)$$

where  $f_i$  and  $g_i$  are the distribution functions, with  $f_i^{eq}$  and  $g_i^{eq}$  being the corresponding equilibrium distribution functions; subscript  $i$  is the discrete direction of the lattice velocity  $\mathbf{c}_i$ ,  $\mathbf{x}$  is lattice position,  $\mathbf{u}$  is velocity vector,  $t$  is time,  $\Delta t$  is the time step,  $\tau_f$  and  $\tau_g$  are the relaxation parameters; the macroscopic variable  $\mathbf{F}$  is the body force,  $\rho$  is the local density,  $\phi = (\rho_1 - \rho_2)/2$  is the order parameter to distinguish two phases with density  $\rho_1$  and  $\rho_2$ ,  $\mu$  is the chemical potential and it is related to the interface tension coefficient  $\sigma$ . The kinematic viscosity  $\nu$  is closely related to the relaxation parameter  $\tau_f$  as

$$\tau_f = \frac{1}{2} + \frac{3\nu}{c^2 \Delta t}, \quad (12)$$

when using the widely adopted lattice velocity model like D2Q9 or D3Q19 in this paper.

Through fluid–fluid interface, which usually covers 3–5 lattice widths, fluid properties such as kinematic viscosity and density are assumed to be linearly proportional to the weight of  $\phi$  as

$$\nu = \nu_1 + \frac{\phi - \phi_1}{\phi_2 - \phi_1} (\nu_2 - \nu_1) \quad (13a)$$

$$\rho = \rho_1 + \frac{\phi - \phi_1}{\phi_2 - \phi_1} (\rho_2 - \rho_1). \quad (13b)$$

This treatment for the transition area has been widely adopted and found to be quite effective (He et al., 1999; Xie et al., 2016a), and it captures the viscous coupling inherently compared with other works that used velocity and stress continuity conditions at prescribed interfaces (Patzek and Kristensen, 2001; Dehghanpour et al., 2011).

By using the Chapman–Enskog expansion, the Navier–Stokes equation

$$\partial_t(\rho \mathbf{u}) + \nabla(\rho \mathbf{u} \mathbf{u}) = -\nabla(\rho_0 c^2/3) + \rho \nu \Delta \mathbf{u} - \phi \nabla \mu + \mathbf{F}, \quad (14)$$

and the convective Cahn–Hilliard equation (Cahn and Hilliard, 1958; Anderson et al., 1998)

$$\partial_t \phi + \mathbf{u} \cdot \nabla \phi = M \nabla^2 \mu \quad (15)$$

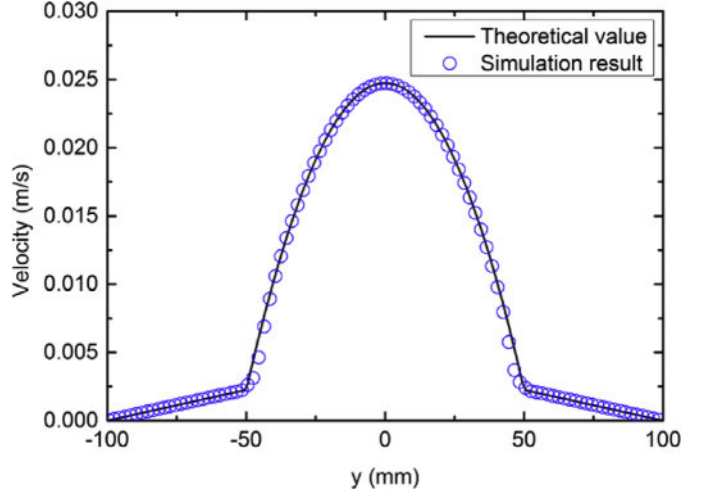


Fig. 3. Cross-sectional velocity profile of the two-phase co-current flow.

can be recovered to second-order accuracy from Eqs. (8) and (9). Here  $\rho_0 = (\rho_1 + \rho_2)/2$  is the mean density, and  $M$  is the mobility controlling the diffusion rate of interface (Huang et al., 2009b). Therefore, this model is successful in dealing with two-phase flows with large density and viscosity ratios, and it is further developed to consider two-phase non-Newtonian fluids (Xie et al., 2016a).

### 3. Results and discussion

In this section, we start with two benchmarks to validate the accuracy of the multiphase LBM model to capture the viscous coupling effect. Then, two-phase flows in triangular tubes are simulated by the LBM. The major two kinds of fluid configurations are discussed, including the water in corner case and the oil in layer case. Next, a pore-network model (Valvatne and Blunt, 2004) is modified by considering this effect using two correction functions. Finally, the effect of the viscous coupling on the pore-network model predictions is investigated.

#### 3.1. Benchmarks

The multiphase LBM code used in this work has been validated in previous works, including test cases considering static and dynamic contact angles for wettability (Xie et al., 2016b), and the Young–Laplace law for capillary pressure (Xie et al., 2016a). In this work, the emphasis is on accurately describing the viscous coupling effect.

In the first test case, the analytical solution for two-phase co-current flow between parallel plates depicted in Fig. 2 is examined. The fluid domain is set as 100 mm × 200 mm × 20 mm on 101 × 201 × 21 lattices with  $H = 200$  mm and  $Y_i = 50$  mm. Periodic boundary conditions are applied on the  $x$  and  $z$  axes, while for the solid boundaries at top and bottom of the  $y$  axis, bounce-back rules are adopted which produce a no-flow boundary condition at the solid wall. Fluid densities are  $\rho_1 = 50$  kg/m<sup>3</sup> and  $\rho_2 = 1000$  kg/m<sup>3</sup>; kinematic viscosities are  $\nu_1 = \nu_2 = 0.01667$  m<sup>2</sup>/s; interface tension is  $\sigma = 0.03$  N/m; mobility is  $M = 0.01$  kg · s/m<sup>3</sup>; and lattice velocity is  $c = 100$  m/s. The applied body forces for this case are set as  $F_1 = 15$  Pa/m and  $F_2 = 0$ , which means that fluid 2 will be dragged by fluid 1 through the viscous shear force at the interfaces. When the system reaches the steady state, we are able to extract the velocity profile in Fig. 3, showing an excellent agreement between our simulation data and the theoretical solution.

The second test case is the simulation of a Poiseuille-type co-current flow with the same geometry as in Fig. 2, but applying a

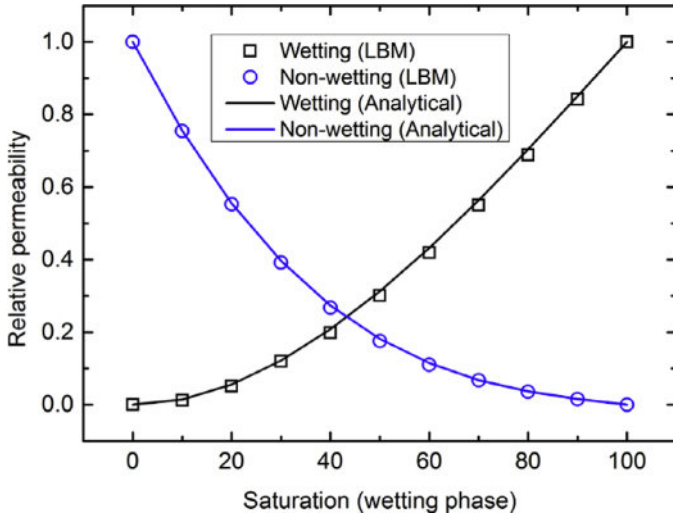


Fig. 4. Relative permeability results for two-phase co-current flow.

uniform pressure gradient (body force) as  $\nabla P_1 = \nabla P_2 = \nabla P$ . For this case, the analytical relative permeability for the wetting fluid 2 and non-wetting fluid 1 are given as (Yiotis et al., 2007)

$$k_{r2} = \frac{1}{2} S_2^2 (3 - S_2) \quad (16a)$$

$$k_{r1} = S_1 \left[ \frac{3}{2} \frac{\rho_1 \nu_1}{\rho_2 \nu_2} + S_1^2 \left( 1 - \frac{3}{2} \frac{\rho_1 \nu_1}{\rho_2 \nu_2} \right) \right], \quad (16b)$$

where  $S_2$  and  $S_1$  are the wetting phase saturation and the non-wetting phase saturation, respectively.

In the following simulation, the computational domain and boundary conditions are the same as in the first case, but the interface position  $Y_i$  is varied to get different saturation configurations. Here  $Y_i = 10 \text{ mm} - 90 \text{ mm}$  are chosen which corresponds to the wetting phase saturations of 90%–10%, respectively. While the other two full saturated ( $S_2 = 100\%$  and 0%) permeability data are simply given by the ordinary single-phase LBM simulations. Fluid densities are different from the first case with  $\rho_1 = 100 \text{ kg/m}^3$  and  $\rho_2 = 1000 \text{ kg/m}^3$ , while the other properties are kept the same. The pressure gradient is set as  $\nabla P = 15 \text{ Pa/m}$ . Thence, the relative permeabilities can be computed as

$$k_{r2}(S_2) = \frac{\int_{|y|=Y_i}^H u_2 dy}{\int_{|y|=0}^H u_{2,SP} dy} \quad (17a)$$

$$k_{r1}(S_2) = \frac{\int_{|y|=0}^{Y_i} u_1 dy}{\int_{|y|=0}^H u_{1,SP} dy}, \quad (17b)$$

when the steady-state velocities  $u_1$  and  $u_2$  are reached.  $u_{1,SP}$  and  $u_{2,SP}$  are the single-phase velocities for fluids 1 and 2 under the same flow conditions. Fig. 4 compares the present LBM results with the analytical results, again, the data match well with each other.

The above two benchmark cases validate the accuracy of our multiphase LBM model to account for viscous coupling effect and to calculate the relative permeability.

### 3.2. Viscous coupling effect on the pore-network prediction

In this subsection, we will use the multiphase LBM model as a direct simulator for flow in pores or throats, to further examine the impact of viscous coupling effect on predicting the transport properties in pore-network models. Two types of fluid configuration in a pore/throat corner are considered. In both cases, fluids are

driven by a uniform pressure gradient perpendicular to the plane and flow through an equilateral triangular tube. The cross-sectional fluid configurations are shown in Figs. 5 and 6, with the blue region representing water, the red region representing oil, and the half angle being  $\beta = 30^\circ$

In our calculations, water density is set to  $\rho_w = 1000 \text{ kg/m}^3$ , oil density is  $\rho_o = 800 \text{ kg/m}^3$ , and the interface tension is set to  $\sigma = 0.01 \text{ N/m}$ . The flow domain size is  $2 \text{ mm} \times 1.74 \text{ mm} \times 0.1 \text{ mm}$  on a  $201 \times 175 \times 11$  lattice with the side length of the equilateral triangle being  $2 \text{ mm}$ . Periodic boundary condition is applied on  $z$  axis which contains 11 lattices along the flow direction, and bounce-back boundaries are applied on the three sides of the triangle. For the water in corner case, the kinematic viscosity of water is fixed at the value of  $\nu_w = 1 \times 10^{-6} \text{ m}^2/\text{s}$ , while the kinematic viscosity of oil increases from the value of  $\nu_o = 1.25 \times 10^{-6} \text{ m}^2/\text{s}$  to infinite to investigate the viscous coupling effect. In order to account for the infinite viscosity of oil, we switch our two-phase simulation in Fig. 5(a) to a single-phase simulation in Fig. 5(b), where the oil is replaced by the solid rock with the corner water region kept the same. However for the oil in layer case, the kinematic viscosity of oil is fixed as  $\nu_o = 4 \times 10^{-6} \text{ m}^2/\text{s}$ , while the water viscosity increases from  $\nu_w = 3.33 \times 10^{-7} \text{ m}^2/\text{s}$  to infinite. Correspondingly, the single-phase simulation in Fig. 6(b) is necessary, where the water is replaced by the solid rock with the layer oil region being the same.

Initially, the fluid regions are segmented by the radius toward the triangle center. Then, without any external forces, the systems will naturally evolve to their equilibrium states due to the wettability differences. Once the equilibrium states establishes, the interface positions will no longer change and a pressure gradient of  $F = 50 \text{ Pa/m}$  along the  $z$  direction is applied to fluids. Meanwhile, the geometrical parameters needed for predicting the transport properties in Eqs. (3) and (4) are determined. Fig. 5(a) shows the equilibrium configuration for the corner water case with a contact angle of  $\theta = 45^\circ$ , and Fig. 6(a) is the equilibrium configuration for the oil layer case with a contact angle of  $\theta = 90^\circ$ . One may note that the layer configuration here is a little bit different from that of the previous paper (Valvatne and Blunt, 2004). In previous work, the curvatures of the oil–water interface on both sides of the layer are the same, which is in agreement with most natural cases that fluids inside the pores are connected. While in this work, it is the contact angle on two sides set to be same but not the curvature. This is because what we consider here is actually a 2D pore with infinite length, which makes the fluids disconnected, and therefore the curvature is only determined by surface wettability. Although this 2D simplification is adopted, it is compatible with the assumption used in the network model.

Thence, we obtain the steady-state velocities and volumetric flow rates for both phases. For the water in corner case, water flow rates are plotted against water-to-oil dynamic viscosity ratio in Fig. 7(a); while for the layer case, oil flow rates are plotted against oil-to-water dynamic viscosity ratio in Fig. 7(b). It should be noted that the zero viscosity ratio points represent the single-phase flow situations, which are obtained by the ordinary single-phase LBM simulations. Also shown in Fig. 7 are the corresponding pore-network predictions by using Eqs. (1), (3) and (4). It is easily observed that these predictive points are quite close to our single-phase LBM results, which demonstrates the assumption in the original pore-network model that flow in each phase is not considered to be affected by the other phase. However, this assumption is not always valid, because the two-phase results deviate largely from the single-phase results, and the deviation increases obviously with the dynamic viscosity ratio in both cases, which are mainly caused by the viscous coupling effect.

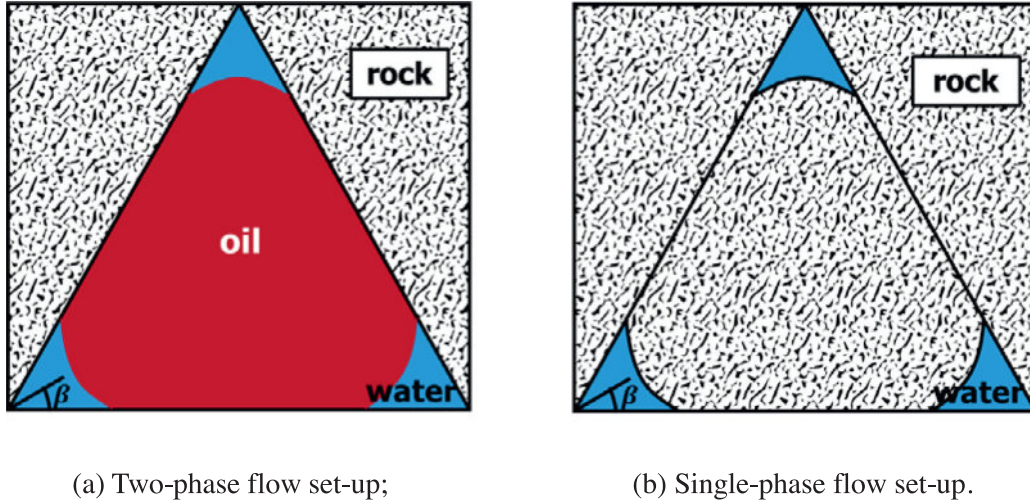


**Fig. 5.** Cross-sectional fluid configuration for water in corner case (half angle  $\beta=30^\circ$ ). (For interpretation of the references to color in this figure, the reader is referred to the web version of this article.)

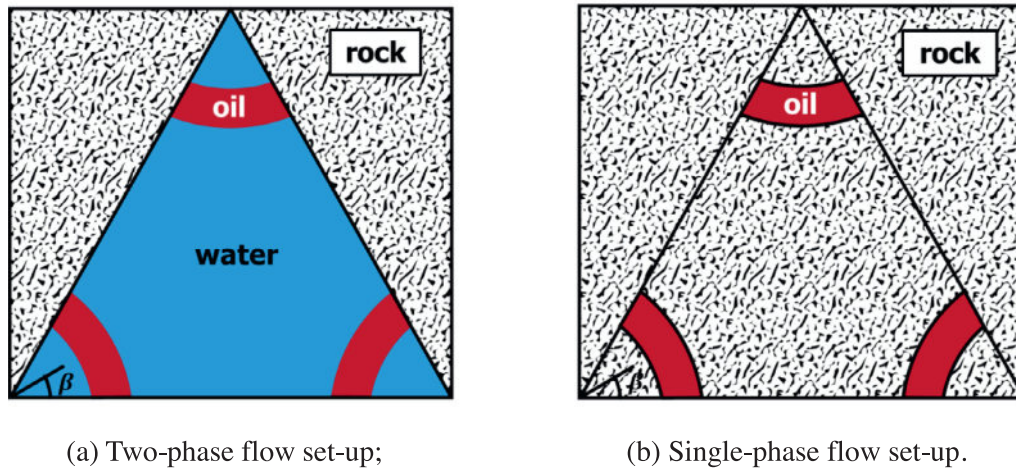


**Fig. 6.** Cross-sectional fluid configuration for oil in layer case (half angle  $\beta=30^\circ$ ). (For interpretation of the references to color in this figure, the reader is referred to the web version of this article.)

In Fig. 8, more detailed information is presented to explain this effect, where we extract velocity profiles along the center line of the cross-sectional triangle. For each configuration, four profiles are obtained under different viscosity ratio conditions including the single-phase condition. From the results, we can see in all regions, the velocities obtained by two-phase simulations are larger than the values obtained by single-phase simulations. For the corner configuration, oil does not move when considered as an infinite-viscosity solid under single-phase condition. However, this is not the case for a real two-phase scenario where the water-to-oil viscosity ratio is not zero. With the increasing of viscosity ratio, oil velocities increase substantially. As a result, the higher-velocity oil will drag the corner water through the viscous shear force at the interface, leading the corner water to gaining more velocity. Similarly, for the oil in layer configuration, due to the effect of viscous coupling, as the oil velocities increase with the oil-to-water viscosity ratio increases. Correspondingly, the higher velocities will lead to much higher flow rates as illustrated in Fig. 7.

In summary, the above results show that the impact of viscous coupling on predicting the transport properties is significant, and the flow of each phase should not be considered independently in the pore-network models.

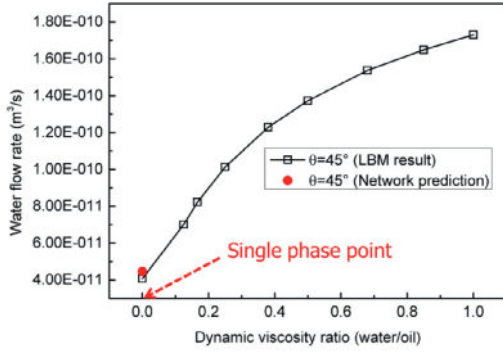
### 3.3. Modification of the pore-network model

The pore-network model by Valvatne and Blunt (Valvatne and Blunt, 2004) is extended considering the viscous coupling effect in this section. From Fig. 7, we observe the monotonous increase of water flow rate in corner with water-to-oil viscosity ratio, and increase of oil flow rate in layer with oil-to-water viscosity ratio. To incorporate this effect in the network model, we add two modification factors  $f_c(\mu_{corner}/\mu_{center})$  and  $f_l(\mu_{layer}/\mu_{corner})$  to the original correlations for the water-film and oil-layer conductance in Eqs. (3) and (4) as

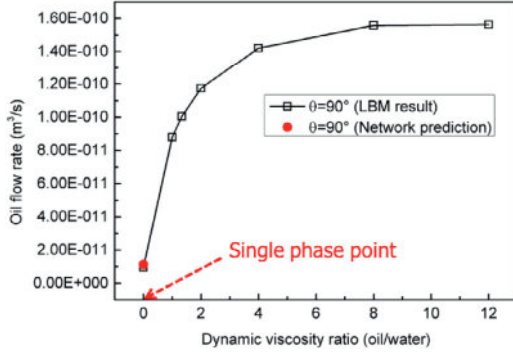
$$g_{p,c} = C \frac{A_c^2 G_c}{\mu_c} \cdot f_c \left( \frac{\mu_{corner}}{\mu_{center}} \right), \quad (18)$$

$$g_{p,l} = \frac{b_o^A \tilde{g}_l}{\mu_l} \cdot f_l \left( \frac{\mu_{layer}}{\mu_{corner}} \right), \quad (19)$$

where the corner function  $f_c(\mu_{corner}/\mu_{center})$  is supposed to be mainly related to the viscosity ratio of fluid in the corner to fluid in the center; while the layer function  $f_l(\mu_{layer}/\mu_{corner})$  is mainly related to the layer-to-corner fluid viscosity ratio. For the zero viscosity ratio conditions, these two functions should be equal to one since the original correlations predict well for the single-phase as illustrated in Fig. 7. Therefore, the two single-phase LBM flow rates



(a) Water in corner case (water flow rate against water-to-oil dynamic viscosity ratio).



(b) Oil in layer case (oil flow rate against oil-to-water dynamic viscosity ratio).

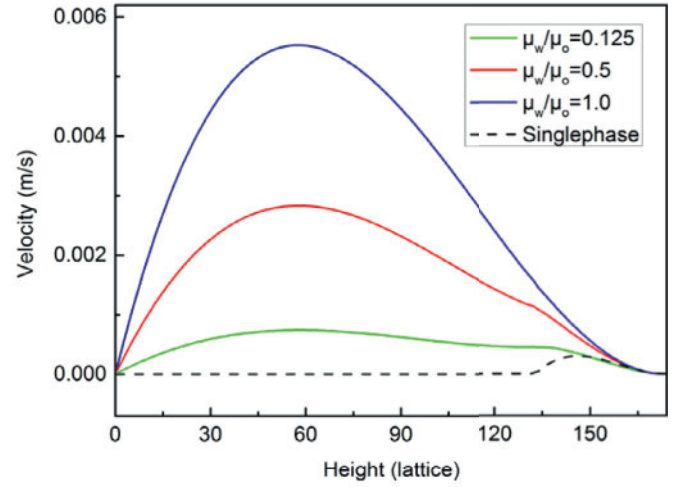
**Fig. 7.** Viscous coupling effect on predicting the flow rates.

are defined as the base rates, and the correction factors for other viscosity ratios are then obtained by dividing the flow rates under two-phase conditions by the base rates.

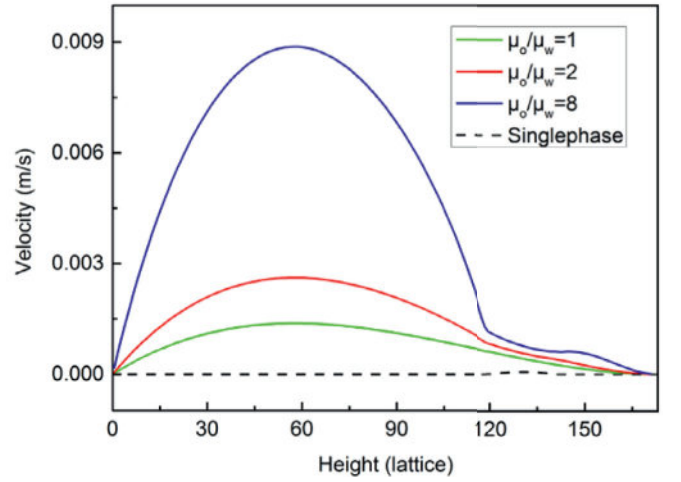
The obtained correction factors as a function of viscosity ratios are shown by the points in Fig. 9. Besides of the two examples in Fig. 7, we also included the impact of contact angle and fluid saturation. For the corner case, contact angles of  $\theta=45^\circ$ ,  $\theta=70^\circ$  and  $\theta=90^\circ$ , with corner water saturation being  $S_w=0.185$ ,  $S_w=0.273$  and  $S_w=0.415$  are discussed. For the layer case, contact angles of  $\theta=90^\circ$ ,  $\theta=110^\circ$  and  $\theta=125^\circ$ , with layer oil saturation being  $S_o=0.168$ ,  $S_o=0.200$  and  $S_o=0.296$  are discussed. These parameter value ranges come from real typical applications. The results indicated that the correction factor was not sensitive to wettability or saturation in these value ranges of properties. This is because the correction factors are the relative ratios between the flow rate predicted under two-phase condition and that under single-phase condition, which scale similarly as contact angle or fluid saturation changes. We believe that the correction factor will show its dependence on wettability and saturation at the extreme values of contact angle and saturation. But for their common values in practice, we can just simplify the correlations as Eqs. (18) and (19) with no dependence on wetting and saturation parameters. By the way, when the contact angle or the saturation is away from the common values, too high or too low, the viscous coupling effect will diminish so that the correction factor will not be so important any more. Thus, two global exponential fitting curves are adopted to fit the scattered data as shown in Fig. 9, which are taken as the empirical modification functions in Eqs. (18) and (19) respectively as

$$f_c(\mu_{corner}/\mu_{center}) = 4.568 - 3.592e^{-1.877 \cdot \frac{\mu_{corner}}{\mu_{center}}} \quad (20)$$

$$f_l(\mu_{layer}/\mu_{corner}) = 16.732 - 15.648e^{-0.925 \cdot \frac{\mu_{layer}}{\mu_{corner}}} \quad (21)$$



(a) Water in corner case.



(b) Oil in layer case.

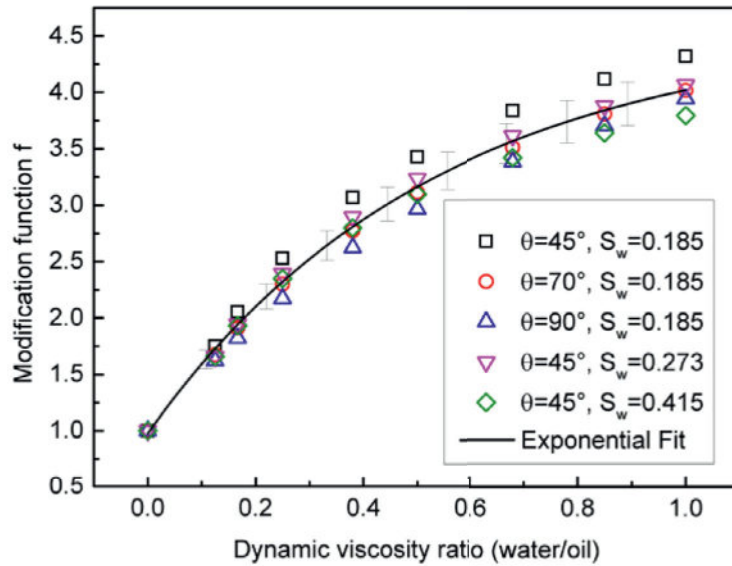
**Fig. 8.** Fluid velocities along the triangle center line. Single-phase results are represented by the dash black lines, and two-phase results under different viscosity ratio conditions are represented by the solid color lines.

Finally, after Eqs. (18)–(21) combined, the original pore-network model is modified for predicting the transport parameters with viscous coupling effect considered.

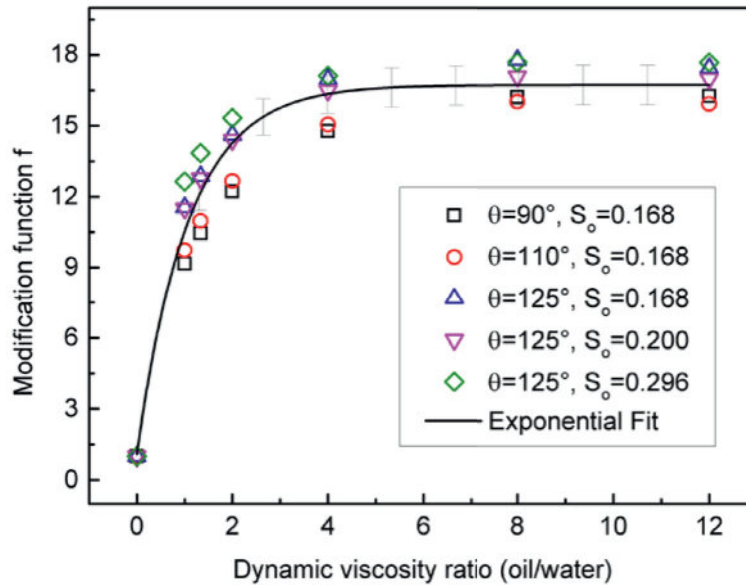
### 3.4. Performance of the modified pore-network model

In this section, the above modification is further examined by revisiting two previous calculations for the relative permeability curves.

The first example is taken from Valvatne's Ph.D. thesis (Valvatne, 2004), where a mixed-wet carbonate "Sample 1" was simulated. This carbonate network was originally modified from a Berea network generated by Bakke and Øren (Bakke and Øren, 1997). Here we keep exact the same parameters as in Valvatne's work, like interface tension (29.9 mN/m), water viscosity ( $0.927 \times 10^{-3}$  Pa/s), oil viscosity ( $6.17 \times 10^{-3}$  Pa/s), water-wet contact angles ( $25^\circ - 65^\circ$ ), oil-wet contact angles ( $80^\circ - 82^\circ$ ) with fraction of 0.68, etc. By using the present model, the relative permeability curves are re-calculated in Fig. 10. Our results are compared with the experimental data (Valvatne, 2004) as well as the original prediction. As is seen, both of the modeling results underpredict the permeabilities, but the results obtained by the modi-



(a) Corner function  $f_c(\mu_{corner}/\mu_{center})$  related to water-to-oil dynamic viscosity ratio.



(b) Layer function  $f_l(\mu_{layer}/\mu_{corner})$  related to oil-to-water dynamic viscosity ratio.

Fig. 9. Modification functions obtained by considering the viscous coupling effect.

fied model are closer to the experiments. This remaining deviation should be mainly ascribed to the network used, which is not originally constructed from the carbonate rock.

Another example is taken from the work of Dong and Blunt (Dong and Blunt, 2009), where the water flooding relative permeabilities for a water-wet Berea sandstone “Sample 13” were predicted. The network was extracted by using an advanced maximal ball algorithm. Again, in the simulation by using the modified pore-network model, all the parameters are kept the same with interface tension being 30 mN/m, water viscosity being  $1.05 \times 10^{-3}$  Pa/s, oil viscosity being  $1.39 \times 10^{-3}$  Pa/s and contact angles being  $50^\circ - 70^\circ$ . The present results are compared with the experimental data (Oak, 1990) and the original predictions, as shown in Fig. 11. The comparisons show evident improvement of the present model over the original model, and good agreement with the experimental data as well. One may find that the im-

provement in this case is better than the previous case, because the effective flow region in homogeneous sandstones is usually larger than that in heterogeneous carbonates, which usually enhances the viscous coupling effect.

Therefore, these results given in the above examples illustrate that the present pore-network model is more accurate due to its pore-scale essence of considering the viscous coupling effect.

#### 4. Conclusions

Using a multiphase LBM model to provide the details of two-phase flow at pore scale, we present an improved pore-network model taking the viscous coupling effect into consideration at core scale. The two-phase LBM simulations in triangular tubes are performed to illustrate the importance of viscous coupling effect in pore-network predictions. Results of two kinds of fluid configura-

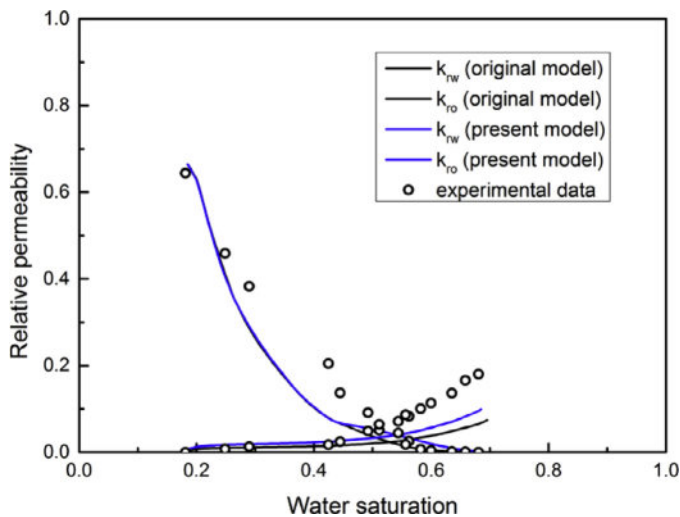


**Fig. 10.** Predicted water flooding relative permeabilities for a mixed-wet carbonate "Sample 1". Present modeling results (blue lines) are compared with the original predictions (black lines). (For interpretation of the references to color in this figure legend, the reader is referred to the web version of this article.)

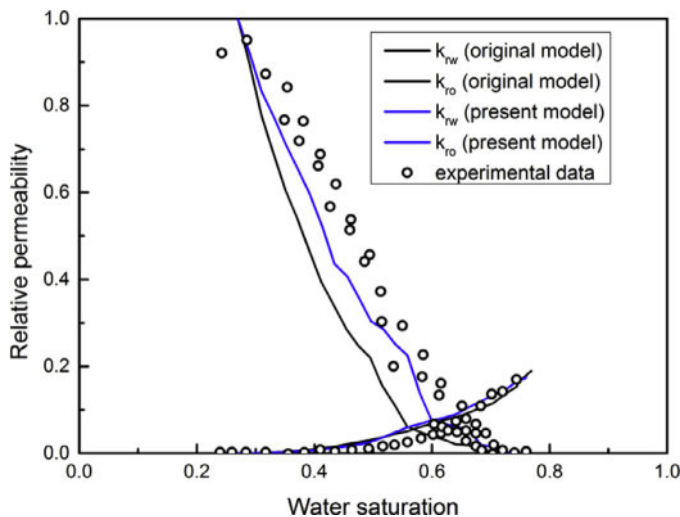


**Fig. 11.** Predicted water flooding relative permeabilities for water-wet Berea sandstone "Sample 13". Present modeling results (blue lines) are compared with the original predictions (black lines). (For interpretation of the references to color in this figure legend, the reader is referred to the web version of this article.)

tions including a water in corner case and an oil layer case indicate that viscous coupling effect have great impact on the fluid velocity distribution and flow rates. We use the LBM results to find correlations for the effect of viscous coupling. The network model is modified by incorporating these correlations as correction factors for water-film and oil conductance. In the end, the accuracy of this improved pore-network model is further validated by revisiting a series of previous predictions for the relative permeability curves.

To conclude, the flow details in pore-scale are usually significant and cannot be neglected, and direct simulations like lattice Boltzmann modeling are able to capture these pore-scale information accurately but they are time consuming, while the pore-network model is extremely efficient and hence practical for larger scale simulations but with less accuracy. This work build the bridge between these two methods, which results to an improved network model containing more pore-scale mechanisms and simultaneously maintaining its original efficiency. We believe the idea of this work could also be extended to developing the pore-

network model by imbedding more complex pore-scale mechanisms, such as wettability characterization, chemical reaction and electrical dynamics.

## Acknowledgments

This work is financially supported by the NSF Grant of China (no. U1562217), National Science and Technology Major Project on Oil and Gas (no. 2017ZX05013001), PetroChina Innovation Foundation (no. 2015D-5006-0201) and the Tsinghua University Initiative Scientific Research Program (no. 2014z22074).

## References

- Ahrenholz, B., Tölke, J., Lehmann, P., Peters, A., Kaestner, A., Krafczyk, M., et al., 2008. Prediction of capillary hysteresis in a porous material using lattice-Boltzmann methods and comparison to experimental data and a morphological pore network model. *Adv. Water Resour.* 31, 1151–1173. <http://dx.doi.org/10.1016/j.advwatres.2008.03.009>.
- Aidun, C.K., Clausen, J.R., 2010. Lattice-Boltzmann method for complex flows. *Annu. Rev. Fluid Mech.* 42, 439–472.
- Anderson, D.M., McFadden, G.B., Wheeler, A.A., 1998. Diffuse-interface methods in fluid mechanics. *Annu. Rev. Fluid Mech.* 30, 139–165.
- Bakke, S., Øren, P.-E., 1997. 3-D pore-scale modelling of sandstones and flow simulations in the pore networks. *SPE J.* 2, 136–149.
- Blunt, M.J., Bijeljic, B., Dong, H., Gharbi, O., Iglauer, S., Mostaghimi, P., et al., 2013. Pore-scale imaging and modelling. *Adv. Water Resour.* 51, 197–216. <http://dx.doi.org/10.1016/j.advwatres.2012.03.003>.
- Blunt, M.J., 2001. Flow in porous media – pore-network models and multiphase flow. *Curr. Opin. Colloid Interface Sci.* 6, 197–207.
- Bryant, S., Blunt, M., 1992. Prediction of relative permeability in simple porous media. *Phys. Rev. A* 46, 2004–2011.
- Bryant, S.L., King, P.R., Mellor, D.W., 1993. Network model evaluation of permeability and spatial correlation in a real random sphere packing. *Transp. Porous Media* 11, 53–70.
- Bryant, S.L., Mellor, D.W., Cade, C.A., 1993. Physically representative network models of transport in porous media. *AIChE J.* 39, 387–396. <http://dx.doi.org/10.1002/aic.690390303>.
- Cahn, J.W., Hilliard, J.E., 1958. Free energy of a nonuniform system. I. Interfacial free energy. *J. Chem. Phys.* 28, 258–267.
- Chen, S., Doolen, G.D., 1998. Lattice Boltzmann method for fluid flows. *Annu. Rev. Fluid Mech.* 30, 329–364.
- Connington, K., Lee, T., 2013. Lattice Boltzmann simulations of forced wetting transitions of drops on superhydrophobic surfaces. *J. Comput. Phys.* 250, 601–615. <http://dx.doi.org/10.1016/j.jcp.2013.05.012>.
- Dehghanpour, H., Aminzadeh, B., DiCarlo, D.A., 2011. Hydraulic conductance and viscous coupling of three-phase layers in angular capillaries. *Phys. Rev. E* 83, 066320.
- Dong, H., Blunt, M.J., 2009. Pore-network extraction from micro-computerized-tomography images. *Phys. Rev. E* 80, 036307. <http://dx.doi.org/10.1103/PhysRevE.80.036307>.
- Ehrlich, R., 1993. Viscous coupling in two-phase flow in porous media and its effect on relative permeabilities. *Transp. Porous Media* 11, 201–218. <http://dx.doi.org/10.1007/bf00614812>.
- Fatt, I., 1956. The network model of porous media. *Pet. Trans. AIME* 207, 144–181.
- Fenwick, D.H., Blunt, M.J., 1998. Network modeling of three-phase flow in porous media. *SPE J.* 3, 86–96.
- Gunstensen, A.K., Rothman, D.H., Zaleski, S., Zanetti, G., 1991. Lattice Boltzmann model of immiscible fluids. *Phys. Rev. A* 43, 4320–4327. <http://dx.doi.org/10.1103/PhysRevA.43.4320>. %/American Physical Society.
- Guo, Y., Wang, M., 2015. Phonon hydrodynamics and its applications in nanoscale heat transport. *Phys. Rep.* 595, 1–44. <http://dx.doi.org/10.1016/j.physrep.2015.07.003>.
- He, X., Li, N., 2000. Lattice Boltzmann simulation of electrochemical systems. *Comput. Phys. Commun.* 129, 158–166. [http://dx.doi.org/10.1016/S0010-4655\(00\)00103-X](http://dx.doi.org/10.1016/S0010-4655(00)00103-X).
- He, X., Chen, S., Zhang, R., 1999. A lattice Boltzmann scheme for incompressible multiphase flow and its application in simulation of Rayleigh–Taylor instability. *J. Comput. Phys.* 152, 642–663. <http://dx.doi.org/10.1006/jcph.1999.6257>.
- Huang, H., Lu, X., 2009. Relative permeabilities and coupling effects in steady-state gas-liquid flow in porous media: a lattice Boltzmann study. *Phys. Fluids* 21, 092104. <http://dx.doi.org/10.1063/1.3225144>.
- Huang, H., Li, Z., Liu, S., Lu, X.-y., 2009. Shan-and-Chen-type multiphase lattice Boltzmann study of viscous coupling effects for two-phase flow in porous media. *Int. J. Numer. Methods Fluids* 61, 341–354.
- Huang, J.J., Shu, C., Chew, Y.T., 2009. Mobility-dependent bifurcations in capillarity-driven two-phase fluid systems by using a lattice Boltzmann phase-field model. *Int. J. Numer. Methods Fluids* 60, 203–225.
- Huang, H., Sukop, M., Lu, X., 2015. Multiphase Lattice Boltzmann Methods: Theory and Application. John Wiley & Sons.
- Inamuro T., Ogata, T., Tajima, S., Konishi, N., 2004. A lattice Boltzmann method for incompressible two-phase flows with large density differences. 198, 628–644.

- Joekar-Niasar, V., Hassanizadeh, S.M., 2012. Analysis of fundamentals of two-phase flow in porous media using dynamic pore-network models: a review. *Crit. Rev. Environ. Sci. Technol.* 42, 1895–1976. <http://dx.doi.org/10.1080/10643389.2011.574101>, Taylor & Francis.
- Lee, T., Lin, C.-L., 2005. A stable discretization of the lattice Boltzmann equation for simulation of incompressible two-phase flows at high density ratio. *J. Comput. Phys.* 206, 16–47. <http://dx.doi.org/10.1016/j.jcp.2004.12.001>.
- Lehmann, P., Berchtold, M., Ahrenholz, B., Tolke, J., Kaestner, A., Krafczyk, M., et al., 2008. Impact of geometrical properties on permeability and fluid phase distribution in porous media. *Adv. Water Resour.* 31, 1188–1204. <http://dx.doi.org/10.1016/j.advwatres.2008.01.019>.
- Li, H., Pan, C., Miller, C.T., 2005. Pore-scale investigation of viscous coupling effects for two-phase flow in porous media. *Phys. Rev. E* 72, 026705.
- Liu, H., Kang, Q., Leonardi, C.R., Jones, B.D., Schmiechek, S., Narváez, A., et al., 2015. Multiphase lattice Boltzmann simulations for porous media applications – a review. *Computational Geosciences* 1–29.
- Mason, G., Morrow, N.R., 1991. Capillary behavior of a perfectly wetting liquid in irregular triangular tubes. *J. Colloid Interface Sci.* 141, 262–274. [http://dx.doi.org/10.1016/0021-9797\(91\)90321-X](http://dx.doi.org/10.1016/0021-9797(91)90321-X).
- Oak M.J. Three-phase relative permeability of water-wet Berea. In: *Proceedings of the SPE/DOE Symposium on Enhanced Oil Recovery*. SPE 20183, 1990.
- Øren, P.-E., Bakke, S., 2003. Reconstruction of Berea sandstone and pore-scale modelling of wettability effects. *J. Pet. Sci. Eng.* 39, 177–199. [http://dx.doi.org/10.1016/S0920-4105\(03\)00062-7](http://dx.doi.org/10.1016/S0920-4105(03)00062-7).
- Oren, P.E., Bakke, S., Arntzen, O.J., 1998. Extending predictive capabilities to network models. *SPE J.* 3, 324–336.
- Patzek, T.W., Kristensen, J.G., 2001. Shape factor correlations of hydraulic conductance in noncircular capillaries. *J. Colloid Interface Sci.* 236, 305–317. <http://dx.doi.org/10.1006/jcis.2000.7414>.
- Patzek, T.W., Silin, D.B., 2001. Shape factor and hydraulic conductance in noncircular capillaries: I. one-phase creeping flow. *J. Colloid Interface Sci.* 236, 295–304. <http://dx.doi.org/10.1006/jcis.2000.7413>.
- Patzek, T.W., 2001. Verification of a complete pore network simulator of drainage and imbibition. *SPE J.* 6, 144–156.
- Piri, M., Blunt, M.J., 2005. Three-dimensional mixed-wet random pore-scale network modeling of two- and three-phase flow in porous media. I. Model description. *Phys. Rev. E* 71, 026301.
- Piri, M., Blunt, M.J., 2005. Three-dimensional mixed-wet random pore-scale network modeling of two- and three-phase flow in porous media. II. Results. *Phys. Rev. E* 71, 026302.
- Raeini, A.Q., Blunt, M.J., Bijeljic, B., 2014. Direct simulations of two-phase flow on micro-CT images of porous media and upscaling of pore-scale forces. *Adv. Water Resour.* 74, 116–126. <http://dx.doi.org/10.1016/j.advwatres.2014.08.012>.
- Ryazanov, A.V., van Dijke, M.I.J., Sorbie, K.S., 2010. Pore-network prediction of residual oil saturation based on oil layer drainage in mixed-wet systems. In: *Proceedings of the Seventeenth SPE Symposium on Improved Oil Recovery SPE 129919-MS2010*.
- Shan, X., Chen, H., 1993. Lattice Boltzmann model for simulating flows with multiple phases and components. *Phys. Rev. E* 47, 1815–1819. <http://dx.doi.org/10.1103/PhysRevE.47.1815>, %/American Physical Society.
- Shao, J.Y., Shu, C., Huang, H.B., Chew, Y.T., 2014. Free-energy-based lattice Boltzmann model for the simulation of multiphase flows with density contrast. *Phys. Rev. E* 89, 033309.
- Swift, M.R., Osborn, W.R., Yeomans, J.M., 1995. Lattice Boltzmann simulation of non-ideal fluids. *Phys. Rev. Lett.* 75, 830–833. <http://dx.doi.org/10.1103/PhysRevLett.75.830>, %/American Physical Society.
- Valvatne, P.H., Blunt, M.J., 2004. Predictive pore-scale modeling of two-phase flow in mixed wet media. *Water Resour. Res.* 40 W07406.
- Valvatne, P.H., Piri, M., Lopez, X., Blunt, M.J., 2005. Predictive pore-scale modeling of single and multiphase flow. *Transp. Porous Media* 58, 23–41.
- Valvatne, P.H., 2004. *Predictive Pore-Scale Modelling of Multiphase Flow*. Imperial College London.
- Van Dijke, M., Sorbie, K.S., Sohrabi, M., Danesh, A., 2004. Three-phase flow WAG processes in mixed-wet porous media: pore-scale network simulations and comparison with water-wet micromodel experiment. *SPE J.* 9, 57–66.
- Vogel, H.J., Tölke, J., Schulz, V.P., Krafczyk, M., Roth, K., 2005. Comparison of a lattice-Boltzmann model, a full-morphology model, and a pore network model for determining capillary pressure-saturation relationships. *Vadose Zone J.* 4, 380–388.
- Wang, M., 2012. Structure effects on electro-osmosis in microporous media. *J. Heat Transf.* 134, 051020.
- Xie, C., Wang, J., Wang, D., Pan, N., Wang, M., 2015. Lattice Boltzmann modeling of thermal conduction in composites with thermal contact resistance. *Commun. Comput. Phys.* 17, 1037–1055.
- Xie, C., Zhang, J., Bertola, V., Wang, M., 2016. Lattice Boltzmann modeling for multiphase viscoplastic fluid flow. *J. Non-Newton. Fluid Mech.* 234, 118–128. <http://dx.doi.org/10.1016/j.jnnfm.2016.05.003>.
- Xie, C., Zhang, J., Bertola, V., Wang, M., 2016. Droplet evaporation on a horizontal substrate under gravity field by mesoscopic modeling. *J. Colloid Interface Sci.* 463, 317–323. <http://dx.doi.org/10.1016/j.jcis.2015.10.054>.
- Yiotis, A.G., Psihogios, J., Kainourgiakis, M.E., Papaioannou, A., Stubos, A.K., 2007. A lattice Boltzmann study of viscous coupling effects in immiscible two-phase flow in porous media. *Colloids Surf. A Physicochem. Eng. Asp.* 300, 35–49. <http://dx.doi.org/10.1016/j.colsurfa.2006.12.045>.
- Zheng, H.W., Shu, C., Chew, Y.T., 2006. A lattice Boltzmann model for multiphase flows with large density ratio. *J. Comput. Phys.* 218, 353–371. <http://dx.doi.org/10.1016/j.jcp.2006.02.015>.